MCB
Journals.ASM.org

A Regulatory Role for MicroRNA 33* in Controlling Lipid Metabolism Gene Expression

Leigh Goedeke,[a] Frances M. Vales-Lara,[a] Michael Fenstermaker,[a] Daniel Cirera-Salinas,[a] Aranzazu Chamorro-Jorganes,[a] Cristina M. Ramírez,[a] Julie A. Mattison,[b] Rafael de Cabo,[b] Yajaira Suárez,[a] Carlos Fernández-Hernando[a]

Department of Medicine, Leon H. Charney Division of Cardiology, Department of Cell Biology, and the Marc and Ruti Bell Vascular Biology and Disease Program, New York University School of Medicine, New York, New York, USA[a]; Translational Gerontology Branch, National Institute on Aging, National Institutes of Health, Baltimore, Maryland, USA[b]

hsa-miR-33a and hsa-miR-33b, intronic microRNAs (miRNAs) located within the sterol regulatory element-binding protein 2 and 1 genes (*Srebp-2* and *-1*), respectively, have recently been shown to regulate lipid homeostasis in concert with their host genes. Although the functional role of miR-33a and -b has been highly investigated, the role of their passenger strands, miR-33a* and -b*, remains unclear. Here, we demonstrate that miR-33a* and -b* accumulate to steady-state levels in human, mouse, and nonhuman primate tissues and share a similar lipid metabolism target gene network as their sister strands. Analogous to miR-33, miR-33* represses key enzymes involved in cholesterol efflux (ABCA1 and NPC1), fatty acid metabolism (CROT and CPT1a), and insulin signaling (IRS2). Moreover, miR-33* also targets key transcriptional regulators of lipid metabolism, including SRC1, SRC3, NFYC, and RIP140. Importantly, inhibition of either miR-33 or miR-33* rescues target gene expression in cells overexpressing pre-miR-33. Consistent with this, overexpression of miR-33* reduces fatty acid oxidation in human hepatic cells. Altogether, these data support a regulatory role for the miRNA* species and suggest that miR-33 regulates lipid metabolism through both arms of the miR-33/miR-33* duplex.

MicroRNAs (miRNAs) are an abundant class of endogenous noncoding RNAs that have emerged as key posttranscriptional regulators of gene expression (1). In animals, miRNAs cause repression by base pairing to the 3′ untranslated region (3′ UTR) of their target mRNAs, which contain perfect or near-perfect sequence complementarity to nucleotides (nt) 2 to 8 (the "seed region") of the mature miRNA (1–3). The canonical miRNA biogenesis pathway involves the stepwise processing of primary miRNA transcripts (pri-miRNAs) by the RNase III proteins Drosha and Dicer (1–3). After processing by Drosha in the nucleus, the pri-miRNA is exported to the cytoplasm and subsequently cleaved by Dicer to produce an ~22-nt miRNA/miRNA* duplex (1–3). Although both strands of the duplex are necessarily produced in equal amounts by transcription, their accumulation is asymmetric at the steady state (4–6). By convention, the most abundant duplex strand is defined as the mature miRNA strand, whereas the less abundant strand is known as the "passenger strand," or miRNA star strand (herein referred to as miRNA*) (4, 5, 7). The mechanisms of miRNA strand selection and RNA-induced silencing complex (RISC) loading are still unclear; however, it is thought that strand selection is dictated by the relative thermodynamic stability of each duplex end (4, 5). The strand with unstable base pairs at the 5′ end typically evades degradation and is incorporated into Argonaute (Ago) complexes, where it mediates posttranscriptional gene silencing (4, 5).

Although miRNAs have been implicated in numerous normal and disease-related biological processes, the potential regulatory activity of the miRNA* species is less well known. Nonetheless, it has been shown that a substantial fraction of *Drosophila melanogaster* miRNA genes are highly conserved along both miRNA and miRNA* strands and that abundant miRNA* species are present at physiologically relevant levels and can associate with Argonaute proteins (8). While most *Drosophila* miRNAs are bound to Ago1 (9), the passenger strand is bound to the small interfering RNA (siRNA) effector Ago2 (10–12) and exerts a detectable impact on gene regulatory networks in this species. With the development of deep sequencing technologies, a similar functionality for vertebrate miRNA* species is now emerging (13–15). In particular, recent groups have demonstrated not only the significant presence of miRNA* strands across species, but their regulatory role as well (16, 17).

Profiling approaches from our group and others aimed at identifying miRNAs that regulate cholesterol homeostasis discovered the presence of miR-33a and -b in the introns of the sterol regulatory element-binding protein (SREBP) genes *Srebp-1* and *Srebp-2* (18, 19). These loci code for the membrane-bound transcription factors SREBP-1 and SREBP-2, which modulate the transcription of a number of genes involved in the synthesis and receptor-mediated uptake of cholesterol and fatty acids (20). During conditions of low intracellular cholesterol, miR-33a is cotranscribed with *Srebp-2* and works to increase cellular cholesterol levels by reducing cholesterol export through the inhibition of the ATP binding cassette (ABC) transporters ABCA1 and ABCG1, as well as the endolysosomal protein Niemann-Pick C1 (NPC1) (18, 19, 21, 22). Similarly, when *Srebp-1c* is induced during hyperinsulinemia or insulin resistance, miR-33b is cotranscribed and

Received 18 December 2012 **Returned for modification** 12 January 2013
Accepted 25 March 2013

Published ahead of print 1 April 2013

Address correspondence to Carlos Fernández-Hernando, carlos.fernandez-hernando@nyumc.org.

Supplemental material for this article may be found at http://dx.doi.org/10.1128/MCB.01714-12.

doi:10.1128/MCB.01714-12

works to reduce cellular fatty acid oxidation by targeting carnitine *O*-octanoyltransferase (CROT), carnitine palmitoyltransferase 1A (CPT1a), hydroxyacyl coenzyme A (hydroxyacyl-CoA) dehydrogenase subunit beta (HADHB), and AMP kinase subunit alpha (AMPKα), as well as insulin signaling, by targeting insulin receptor substrate 2 (IRS2) and sirtuin 6 (SIRT6) (23, 24). In addition, we and others have recently shown that miR-33 contributes to the regulation of cholesterol and fatty acid homeostasis by targeting key transcriptional regulators of lipid metabolism, including steroid receptor coactivator 1 (SRC1), steroid receptor coactivator 3 (SRC3), nuclear transcription factor Y, gamma (NFYC), and nuclear receptor-interacting protein 1 (RIP140) (25).

While the functional role of miR-33 has been highly investigated, the role of its passenger strand, miR-33*, has not been addressed. Here, we report that miR-33* is highly conserved across animal species and accumulates to steady-state levels in human, mouse, and nonhuman primate tissues. Additionally, we demonstrate that miR-33* shares a similar target network to miR-33 and directly represses target genes in human hepatic and macrophage cell lines. Importantly, inhibition of either miR-33 or miR-33* rescues target gene expression in human hepatic cells overexpressing pre-miR-33. Consistent with this and in support of a physiological role for the miR-33* species, miR-33* overexpression reduces fatty acid oxidation in hepatocytes. Altogether, these data support a regulatory role for the miRNA* species and suggest that miR-33 regulates lipid metabolism through both arms of the miR-33/miR-33* duplex.

MATERIALS AND METHODS

Materials. Chemicals were obtained from Sigma unless otherwise noted. The synthetic LXR ligand T0901217 was purchased from Cayman Chemical. Total human RNA was purchased from Life Technologies (FirstChoice human total RNA survey panel). Mouse monoclonal antibodies against ABCA1 and Dicer were purchased from Abcam. Rabbit polyclonal antibodies against NPC1 and CROT, a mouse monoclonal antibody against NFYC, and a goat polyclonal antibody against CPT1a were obtained from Novus. A rabbit polyclonal antibody against IRS2 was purchased from Bethyl, and a rabbit polyclonal antibody against RIP140 was acquired from Santa Cruz. Rabbit polyclonal antibodies against SRC1 and SRC3 were purchased from Cell Signaling, and a mouse monoclonal antibody against heat shock protein 90 (HSP90) was obtained from BD Biosciences. Secondary fluorescently labeled antibodies were from Molecular Probes (Invitrogen).

Bioinformatic analysis. Target genes for miR-33a, miR-33a*, miR-33b, and miR-33b* were identified and compared using the online target prediction algorithm miRWalk, which provides target interaction information from eight different prediction programs. Specifically the programs miRanda, miRDB, miRWalk, and TargetScan were used. Putative targets produced by at least two of the programs for miR-33a (7,245 targets) and miR-33b (5,891 targets) and at least one of the programs for miR-33a* (4,488 targets) and miR-33b* (4,692 targets) were then uploaded into Reactome (www.reactome.org) to find significantly enriched pathways.

Cell culture. Human hepatic (Huh7), human monocytic (THP1), and monkey kidney fibroblast (COS7) cells were obtained from American Type Culture Collection. Huh7 and COS7 cells were maintained in Dulbecco's modified Eagle's medium (DMEM) containing 10% fetal bovine serum (FBS) and 2% penicillin-streptomycin in 10-cm^2 dishes at 37°C and 5% CO_2. THP1 cells were maintained in RPMI 1640 medium (Sigma) supplemented with 10% FBS and 2% penicillin-streptomycin. THP1 differentiation into macrophages was induced using 100 nM phorbol-12-myristate acetate (PMA) for 72 h. For analysis of miR-33a and -a* expression, Huh7 cells were plated in DMEM containing 10% lipoprotein-deficient serum (LPDS) and treated with native low-density lipoprotein (nLDL; 120 μg/ml) or simvastatin (5 μM) for 24 h. For analysis of miR-33b and -b* expression, Huh7 cells were plated in DMEM containing 10% FBS and stimulated with 10 μM T090 for 12 h.

RNA isolation and qRT-PCR. Total RNA was isolated using TRIzol reagent (Invitrogen) according to the manufacturer's protocol. For mRNA quantification, cDNA was synthesized using iScript RT supermix (Bio-Rad), following the manufacturer's protocol. Quantitative real-time PCR (qRT-PCR) was performed in triplicate using iQ SYBR green supermix (Bio-Rad) on an iCycler real-time detection system (Bio-Rad). The mRNA level was normalized to the gene coding for GAPDH (glyceraldehyde-3-phosphate dehydrogenase) or 18S as a housekeeping gene. The following human primer sequences were used: 18S, 5′-AGCTATCAATC TGTCAATCCTGTC-3′ and 5′-GCTTAATTTGACTCAACACGGGA-3′; ABCA1, 5′-GGTTTGGAGATGGTTATACAATAGTTGT-3′ and 5′-CCC GGAAACGCAAGTCC-3′; GAPDH, 5′-AACTTTGGCATTGTGGAAG G-3′ and 5′-ACACATTGGGGGTAGGAACA-3′; SRC1, 5′-ACCACTTT GTCTGTCGAGCCTGA-3′ and 5′-TCCAGGCTCAGGTTTGGAGTTG AT-3′; SRC3, 5′-ATGCCACAGGCCTGGAAGAAATTG-3′ and 5′-CTG CTTCTTGGCCTTGGAAAGCAT-3′; NFYC, 5′-GACACTTGCCACCA ATGCTCAACA-3′ and 5′-AGAGCTGCTGTCCATCTGTGAACT-3′; RIP140, 5′-AGGGAGGCTTCATCTGCTGAAAGT-3′ and 5′-AACTTCT CCATTTGCGCTGTGTGG-3′; NPC1, 5′-CTTAGTGCAGGAACTCTG TCCAGG-3′ and 5′-TCCACATCACGGCAGGCATTGTAC-3′; IRS2 5′-ACCTCAGTTCAAGGTAAAGCCGGA-3′ and 5′-AGGTACCTGCACT GGAATCCAACA-3′; CPT1a, 5′-TGCTTTACAGGCGCAAACTG-3′ and 5′-TGGAATCGTGGATCCCAAA-3′; CROT, 5′-TGTTCACCACAG GGATACAAGCCT-3′ and 5′-TACCTTGGCCTCCCACCGTGCTAA-3′; SREBP-1c, 5′-TCAGCGAGGCGGCTTTGGAGCAG-3′ and 5′-CATG TCTTCGATGTCGGTCAG-3′; and SREBP-2, 5′-AACGGTCATTCACCC AGGTC-3′ and 5′-GGCTGAAGAATAGGAGTTGCC-3′. The following mouse primer sequences were used: SREBP-2, 5′-GCGTTCTGGAGACC ATGGA-3′ and 5′-ACAAAGTTGCTCTGAAAACAAATCA-3′; and 18S, 5′-TTCCGATAACGAACGAGACTCT-3′ and 5′-TGGCTGAACGCCAC TTGTC-3′. The following monkey primer sequences were used: SREBP-1c, 5′-CAACGCTGGCCGAGATCTAT-3′ and 5′-TCCCCATCCACGAA GAAACG-3′. For miRNA quantification, total RNA was reverse transcribed using the RT^2 miRNA First Strand kit (SABiosciences) or miScript II RT kit (Qiagen). Primers specific for human miR-33a, miR-33a*, miR-33b, and miR-33b* (SABiosciences) or miR-33a, miR-33a*, miR-33b, miR-33b*, miR-451, and miR-148a (Qiagen) were used, and values were normalized to either of the SNORD38B (SABiosciences) or SNORD68 (Qiagen) housekeeping genes.

miRNA transfection. Huh7 and THP1 cells were transfected with 40 nM mi*RIDIAN* miRNA mimic (miR-33a, mIR-33b, miR-33a*, or miR-33b*) or with 60 nM mi*RIDIAN* miRNA inhibitor (Inh-miR-33a, Inh-miR-33a*, Inh-miR-33b, or Inh-miR-33b*) (Dharmacon) utilizing RNAiMax (Invitrogen). All experimental control samples were treated with an equal concentration of a nontargeting control mimic (CM) sequence (Dharmacon) or inhibitor negative-control sequence (CI) (Dharmacon) to control for non-sequence-specific effects in miRNA experiments. Verification of miR-33 and -33* overexpression and inhibition was determined using qRT-PCR as described above.

Lentivirus and Huh7 transduction. A lentivirus encoding the miR-33a precursor (miR-33) and empty vector control were obtained from System Biosciences, Inc. (SBI). High-titer preparations were produced by vector gene transfer (University of Iowa) (18). Subconfluent cultures of Huh7 cells were infected with 3×10^6 lentiviral particles from empty vector or miR-33 for 16 h. The medium then was replaced, and after 48 h, the cells were split and treated 24 h later with lentiviral particles as previously described (26). Forty-eight hours after the last treatment, the efficiency of transduction was confirmed via flow cytometry and immunofluorescence by measuring green fluorescent protein (GFP) expression as described below.

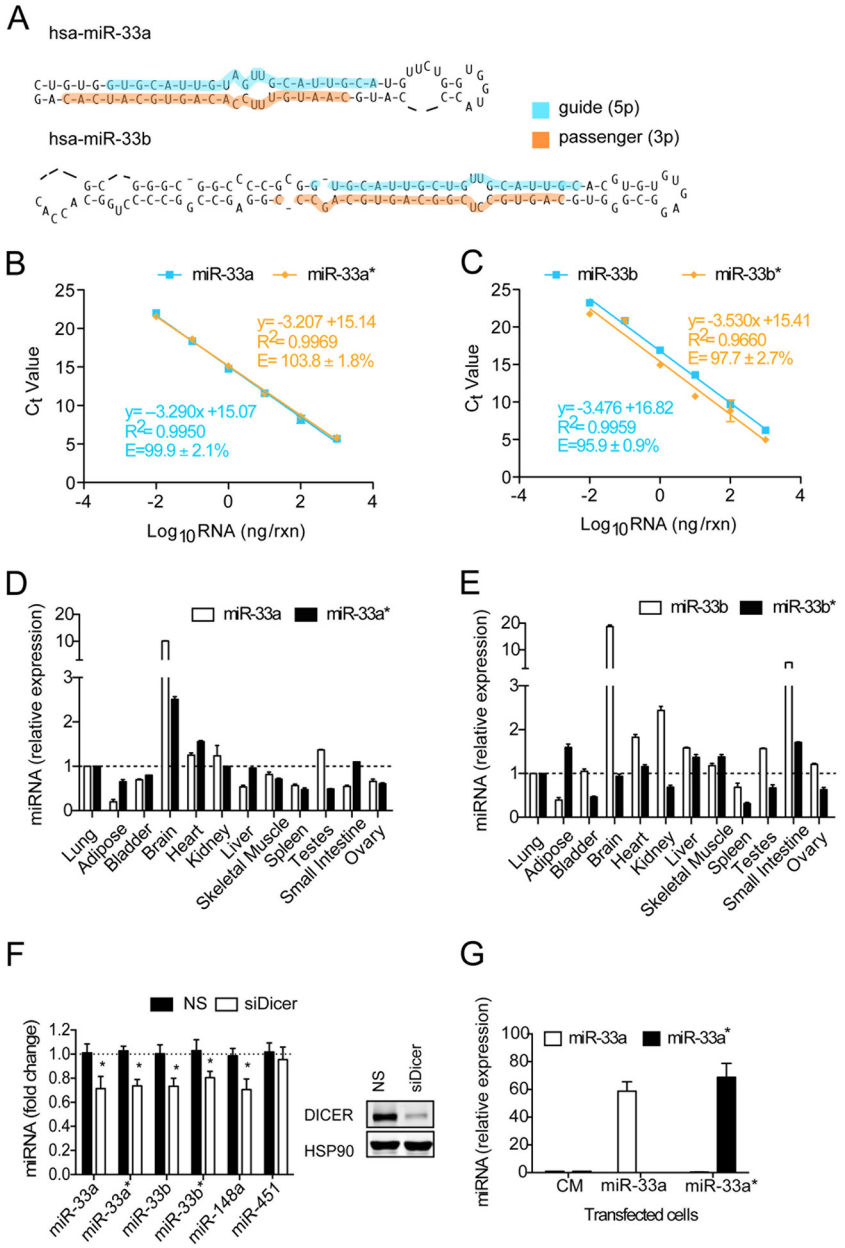

FIG 1 miR-33a and -a* and miR-33b and -b* are differentially expressed in human tissues. (A) Schematic representation of hsa-miR-33a and hsa-miR-33b stem-loop structures. Mature sequences for the 5′ (5p) and 3′ (3p) strands are highlighted in blue and orange, respectively. (B) Assessment of miR-33a and miR-33a* primer efficiencies. Cycle threshold (C_t) values were plotted against the log of six sequential 10-fold dilutions of human miR-33a or -33a* mimics. Efficiency (E) = 10(−1/slope). (C) Assessment of miR-33b and miR-33b* primer efficiencies. Cycle threshold values were plotted against the log of six sequential 10-fold dilutions of human miR-33b or -33b* mimics. E = 10(−1/slope). (D) Expression profile of miR-33a and miR-33a* in selected human tissues (Life Technologies). (E) Expression profile of miR-33b and miR-33b* in selected human tissues (Life Technologies). (F) qRT-PCR analysis of miR-33a, miR-33a*, miR-33b, miR-33b*, miR-148a, and miR-451 in Huh7 cells transfected with nonsilencing control siRNA (NS) or Dicer siRNA (siDicer). Western blot analysis of Dicer expression is shown in the right panel. (G) Assessment of miR-33a and miR-33a* relative expression levels in Huh7 cells transfected with control mimic (CM), miR-33a, or miR-33a* after Ago2 immunoprecipitation (Ago2-IP). The relative expression levels of miR-33a and miR-33a* were normalized to cells transfected with CM. In panels D, E, and G, data are means ± SEM and representative of 2 experiments in duplicate. In panel F, data are means ± SEM from 3 experiments in triplicate. *, $P \leq 0.05$.

Flow cytometry. Huh7 cells were analyzed for expression of GFP by fluorescence flow cytometry. Briefly, monolayers were washed twice in 1× phosphate-buffered saline (PBS) and then incubated with trypsin for 3 min. Enzyme activity was then quenched with 10% FBS–DMEM, and suspended cells were collected and washed in 10 ml cold 1% bovine serum albumin (BSA) (Sigma)–PBS, centrifuged, and washed again in cold 1% BSA–PBS. Cells were then analyzed on a flow cytometer system (Accuri Cytometers) and gated at 10,000 viable cells per sample.

Immunofluorescence. The expression of GFP in empty vector and pre-miR-33-transduced Huh7 cells was analyzed directly using a Zeiss Axiovert 2000 M fluorescence microscope (Carl Zeiss). Images were acquired using a charge-coupled device AxioCam MRm with a 40× objec-

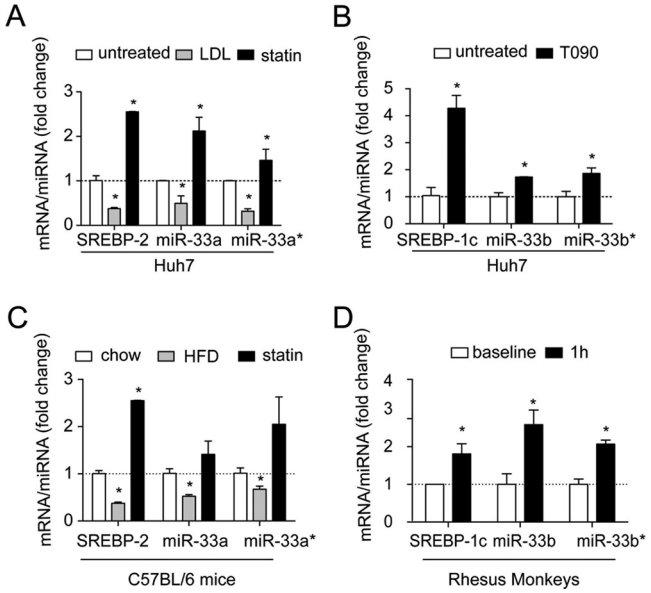

FIG 2 miR-33a and -a* and miR-33b and -b* are coexpressed with their host genes, *Srebp-2* and *Srebp-1*. (A) Quantitative real-time fluorescence PCR (qRT-PCR) analysis of miR-33a, miR-33a*, and SREBP-2 in human hepatic (Huh7) cells loaded with cholesterol by nLDL (120 μg/ml) and depleted of cholesterol by statin treatment (5 μM). (B) qRT-PCR analysis of miR-33b, miR-33b*, and SREBP-1c in Huh7 cells treated with the LXR agonist T0901317 (T090) for 12 h. (C) qRT-PCR analysis of SREBP-2 and miR-33a and miR-33a* in the livers of C57BL6 mice ($n = 5$ per group) fed a chow diet, high-fat diet (HFD), or rosuvastatin-supplemented diet (statin). (D) qRT-PCR analysis of SREBP-1c, miR-33b, and miR-33b* in the livers of rhesus monkeys ($n = 6$ per treatment) after 1 h of glucose stimulation. In panels A to D, the data are means ± SEM and representative of ≥2 experiments in triplicate. *, $P \leq 0.05$.

tive (Carl Zeiss). For lipid droplet analysis, Huh7 cells were transfected with control mimic (CM), miR-33a mimic, or miR-33a* mimic as described above. Following 36 h of transfection, cells were incubated with 1 mM oleate for 12 h and starved for the next 24 h. Cells were washed and fixed for 30 min with 4% paraformaldehyde (PFA)–PBS and stained for 30 min with 1 μg/ml Bodipy 493/503 in PBS. The coverslips were then mounted on glass slides with Gelvato-DAPI (4′,6-diamidino-2-phenylindole) and analyzed using an EVOS$_{fl}$ digital inverted microscope (AMG; batch no. B2112-155D-028; software revision, 9978). Images were acquired using a 20× LPlan FL (AMEP-4624) objective and edited using Photoshop (Adobe).

Lipid content analysis. For lipid quantification, Huh7 cells were transfected with 40 nM control mimic (CM), miR-33a mimic, miR-33a*, or miR-33a and miR-33a* mimic as described above. Following 36 h of transfection, cells were incubated with 1 mM oleate for 12 h and starved for the next 24 h. The cells were then washed three times in 1× PBS and collected; β-hydroxybutyrate, free fatty acids (FFA), and triglycerides were quantified using commercially available kits (Biovision) according to the manufacturers' instructions.

Western blot analysis. Cells were lysed in ice-cold buffer containing 50 mM Tris-HCl (pH 7.5), 125 mM NaCl, 1% NP-40, 5.3 mM NaF, 1.5 mM NaP, 1 mM orthovanadate, 175 mg/ml octylglucopyranoside, 1 mg/ml protease inhibitor cocktail (Roche), and 0.25 mg/ml AEBSF [4-(2-aminoethyl) benzenesulfonyl fluoride hydrochloride] (Roche). Cell lysates were rotated at 4°C for 1 h before the insoluble material was removed by centrifugation at 12,000 × *g* for 10 min. After normalization for equal protein concentration, cell lysates were resuspended in SDS sample buffer before separation by SDS-PAGE. Following overnight transfer of the proteins onto nitrocellulose membranes, the membranes were probed with the antibodies to the following proteins: ABCA1 (1:1,000), NPC1 (1:1,000), IRS2 (1:500), CPT1a (1:500), CROT (1:500), RIP140 (1:500), SRC1 (1:250), SRC3 (1:250), NFYC (1:500), and HSP90 (1:1,000). Protein bands were visualized using the Odyssey infrared imaging system (LI-COR Biotechnology). Densitometry analysis of the gels was carried out using ImageJ software from the NIH (http://rsbweb.nih.gov/ij/).

3′-UTR luciferase reporter assays. cDNA fragments corresponding to the 3′ UTR of ABCA1, NPC1, CROT, IRS2, SRC1, SRC3, and NFYC were amplified by RT-PCR from total RNA extracted from HepG2 cells with XhoI and NotI linkers. The PCR product was directionally cloned downstream of the *Renilla* luciferase open reading frame of the psi-CHECK2 vector (Promega), which also contains a constitutively expressed firefly luciferase gene, which is used to normalize transfections. A cDNA fragment corresponding to the entire 3′ UTR of CPT1a was purchased from GeneCopeia. Point mutations in the seed region of predicted miR-33a* or miR-33b* sites within the 3′ UTR of the above constructs were generated using Multisite-Quickchange (Stratagene) according to the manufacturer's protocol. All constructs were confirmed by sequencing. COS7 cells were plated into 12-well plates (Costar) and cotransfected with 1 μg of the indicated 3′-UTR luciferase reporter vectors and 40 nM the miR-33a* or miR-33b* mimic or negative-control mimic (CM) (Dharmacon) using Lipofectamine 2000 (Invitrogen). Luciferase activity was measured using the Dual-Glo luciferase assay system (Promega). *Renilla* luciferase activity was normalized to the corresponding firefly luciferase activity and plotted as a percentage of the control (cells cotransfected with the corresponding concentration of control mimic). Experiments were performed in triplicate and repeated at least three times.

Ago2-IP. Ago2 immunoprecipitation (Ago2-IP) experiments after miR-33a, miR-33a*, and CM overexpression were conducted with Huh7 cells. Briefly, 1×10^7 cells were transfected with 20 nM miR-33a, miR-33a*, or CM using RNAimax for 24 h. After 24 h, cells were collected and subjected to Ago2-IP using the RNA isolation kit for human Ago2 (Wako Chemicals) according to the manufacturer's instructions. The IP pull-down RNA was used to determine the expression levels of miR-33a, miR-33a*, miR-33b, miR-33b*, miR-148a, miR-451, CROT, and NPC1, as described above.

Mouse studies. Male C57BL/6 mice were purchased from Jackson Laboratories (Bar Harbor, ME) and kept under constant temperature and humidity in a 12-h controlled dark/light cycle. Eight-week-old C57BL/6 male mice ($n = 5$ per group) were placed on a chow diet, a high-fat diet (HFD) containing 0.3% cholesterol and 21% (wt/wt) fat (from Dyets, Inc.), or a chow diet containing 0.005% (wt/wt) rosuvastatin (AstraZeneca UK, Ltd.), equaling 5 mg/kg body weight per day for 3 weeks. At sacrifice, liver samples were collected, snap-frozen, and stored at −80°C. Total liver RNA was isolated using the Bullet blender homogenizer (Next Advance) in TRIzol. One microgram of total RNA was reverse transcribed using the RT^2 miRNA First Strand kit (SABiosciences) for

TABLE 1 Predicted lipid metabolism target genes for miR-33a*

Gene product	Target gene predicted by algorithm[a]		Conserved in mice
	miRanda	miRWalk	
ABCA1	X		Yes
NPC1	X		Yes
CROT	X		No
CPT1a	X	X	Yes
AMPKα	X	X	Yes
IRS2	X		Yes
SRC1	X	X	No
SRC3		X	Yes
RIP140	X	X	Yes
NFYC		X	Yes

[a] X, predicted binding site present.

TABLE 2 Predicted lipid metabolism target genes for miR-33b*

Gene product	Target gene predicted by algorithm[a]		Conserved in mice
	miRanda	miRWalk	
ABCA1	X	X	No
CS	X		No
SRC3	X		No
RIP140	X		No
NFYC	X		No

[a] X, predicted binding site present.

miR-33a and -a* and miR-33b and -b* quantification and normalized to SNORD66 using quantitative PCR described above. For mRNA quantification, cDNA was synthesized using iScript RT supermix (Bio-Rad) and iQ SYBR green supermix (Bio-Rad) as described above. All animal experiments were approved by the Institutional Animal Care Use Committee of New York University Medical Center.

Nonhuman primate studies. Five male rhesus monkeys (*Macaca mulatta*), age 14.3 ± 0.53 years (mean ± standard error of the mean [SEM]), were fasted overnight and anesthetized with ketamine (10 mg/kg); isoflurane gas maintained the anesthesia plane. An ultrasound-guided needle biopsy specimen of the liver was collected at baseline and flash frozen. For the glucose tolerance test (GTT), an intravenous catheter was placed in the saphenous vein. Following the collection of 4 baseline blood samples (3 ml each), a dose of 300 mg/kg of 50% dextrose (Hospire, Inc., Lake Forest, IL) was delivered intravenously (i.v.) over 30 s. Blood samples were then collected at 1, 3, 5, 7, 10, 15, 20, 30, 40, 50, and 60 min after injection. Glucose values were promptly measured in whole blood using an Ascensia Breeze 2 blood glucose monitoring system (Bayer HealthCare LLC., Mishawaka, IN), and additional serum samples were stored at −80°C for subsequent analysis. A second liver biopsy specimen was collected immediately following the 60-min time point and again 6 h after glucose infusion. Animal procedures were approved by the Animal Care and Use Committee of the Biomedical Research Center, National Institute on Aging. Liver RNA was isolated using the Bullet blender homogenizer (Next Advance) in TRIzol. For mRNA quantification, 1 μg of total RNA was reverse transcribed using iScript RT supermix (Bio-Rad) and iQ SYBR green supermix (Bio-Rad). Quantification of miR-33b and miR-33b* was assessed using the RT^2 miRNA First Strand kit (SABiosciences) as described above.

Statistics. All data are expressed as means ± SEM. Statistical differences were measured using either an unpaired Student *t* test or 2-way analysis of variance (ANOVA) with Bonferroni's correction for multiple comparisons when appropriate. A *P* value of ≤0.05 was considered statis-

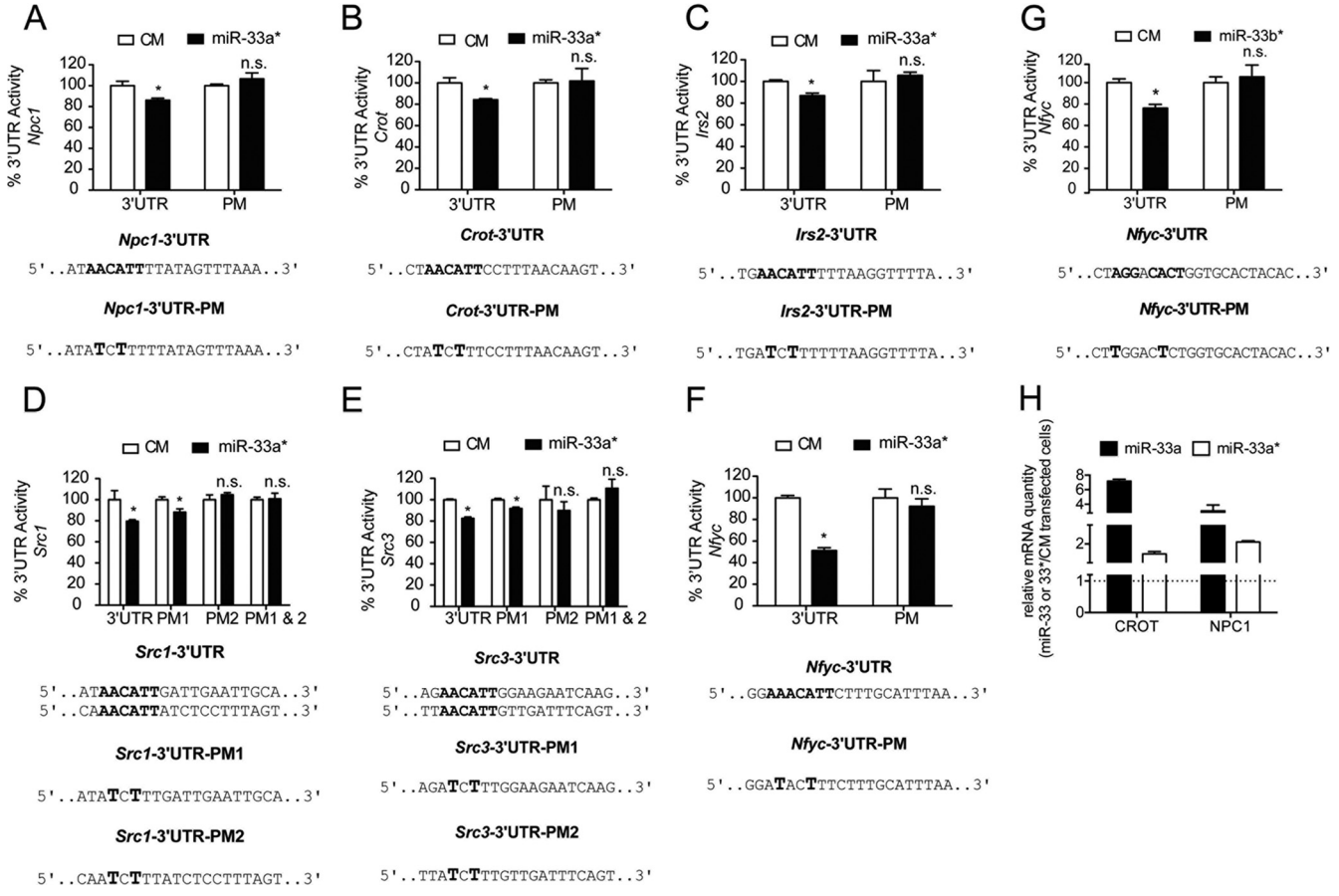

FIG 3 miR-33a* specifically targets the 3′ UTR of human genes *Npc1*, *Crot*, *Irs2*, *Src1*, *Src3*, and *Nyfc*, while miR-33b* specifically targets the 3′ UTR of human *Nyfc*. (A through F) Luciferase reporter activity in COS7 cells transfected with control mimic (CM) or miR-33a* mimic and the human or mouse (A) *Npc1*, (B) *Crot*, (C) *Irs2*, (D) *Src1*, (E) *Src3*, or (F) *Nyfc* 3′ UTRs containing the indicated point mutations (PM) in the miR-33a* target sites. (G) Luciferase reporter activity in COS7 cells transfected with control mimic (CM) or miR-33b* mimic and the human *Nyfc* 3′ UTR containing the indicated point mutations (PM) in the miR-33b* target site. (H) qRT-PCR analysis of CROT and NPC1 in Huh7 cells transfected with the control mimic (CM), miR-33a, or miR-33a* after Ago2 immunoprecipitation (Ago2-IP). In panels A to G, the data are expressed as mean percentages of 3′-UTR activity of CM ± SEM and are representative of ≥3 experiments in triplicate. *, $P \leq 0.05$. n.s., not significant. In panel H, the data are means ± SEM and representative of 2 experiments in duplicate.

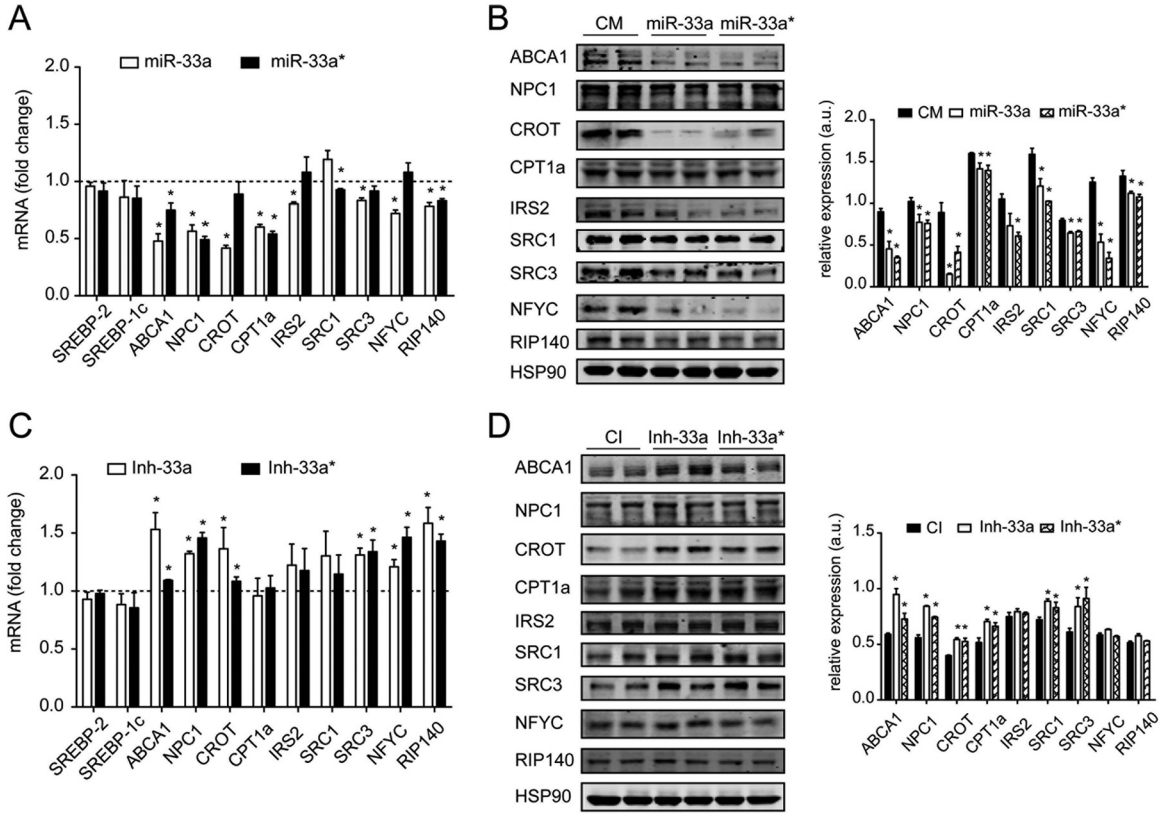

FIG 4 Posttranscriptional regulation of ABCA1, NPC1, CROT, CPT1a, IRS2, SRC1, SRC3, NFYC, and RIP140 by miR-33a and miR-33a* in Huh7 cells. (A) qRT-PCR analysis of SREBP-2, SREBP-1c, ABCA1, NPC1, CROT, CPT1a, IRS2, SRC1, SRC3, NYFC, and RIP140 in Huh7 cells transfected with a control mimic (CM), miR-33a mimic, or miR-33a* mimic. (B) Western blot analysis of ABCA1, NPC1, CROT, CPT1a, IRS2, SRC1, SRC3, NFYC, and RIP140 in Huh7 cells transfected with CM, miR-33a, or miR-33a*. Quantification of protein relative to the loading control (HSP90) is shown in the right panel. a.u., arbitrary units. (C) qRT-PCR analysis of SREBP-2, SREBP-1c, ABCA1, NPC1, CROT, CPT1a, IRS2, SRC1, SRC3, NYFC, and RIP140 in Huh7 cells transfected with a control inhibitor (CI), inhibitor of miR-33a (Inh-33a), or inhibitor of miR-33a* (Inh-33a*). (D) Western blot analysis of ABCA1, NPC1, CROT, CPT1a, IRS2, SRC1, SRC3, NFYC, and RIP140 in Huh7 cells transfected with CI, Inh-33a, or Inh-33a*. Quantification of protein relative to the loading control (HSP90) is shown in the right panel. In panels A to D, the data are means ± SEM and representative of ≥3 experiments in triplicate. *, $P \leq 0.05$.

tically significant. Data analysis was performed using Prism software version 5.0a (GraphPad, San Diego, CA). On the figures, asterisks represent the following: *, $P \leq 0.05$; **, $P \leq 0.01$; and ***, $P \leq 0.001$.

RESULTS

miR-33* is evolutionarily conserved and accumulates to steady-state levels in human, mouse, and nonhuman primate tissues. We previously identified the presence of miR-33 using genome-wide expression profiling in mouse peritoneal macrophages enriched or depleted of cholesterol (18). Interestingly, further characterization of the array revealed that in addition to miR-33, miR-33* (Fig. 1A) was significantly downregulated by cholesterol loading with acetylated-LDL (−1.63-fold change; $P = 0.035$) (27). Recent evidence shows that certain miRNAs display tissue-dependent miRNA arm selection (13), thereby identifying a possible biological function for the accumulation of miRNA* strands. Therefore, after confirming equal primer efficiencies for miR-33a and -a* and miR-33b and -b* (Fig. 1B and C), we first sought to measure the expression of miR-33a and -b and miR-33a* and -b* in various human tissues using qRT-PCR. As seen in Fig. 1D and E, both arms of miR-33 were differentially expressed, especially in the brain, testes, and adipose tissue. Notably, miR-33a* accumulated to higher steady-state levels than miR-33a in the liver, a tissue in which miR-33 has been extensively studied. Our miR-33a* and miR-33b* measurements were specific for the mature form since siRNA-mediated knockdown of Dicer (Fig. 1F, right panel) significantly reduced the expression of both mature miRNAs, while the expression of miR-451, an miRNA that is processed independently of Dicer (28), was unchanged (Fig. 1F, left panel). Similar results were observed when we analyzed the expression of miR-148a, an miRNA highly expressed in human hepatic cell lines (Fig. 1F, left panel). Moreover, to determine the primer specificity for mature miR-33a and -a* and miR-33b and -b* compared to their precursor hairpins, we immunoprecipitated the RISC using an antibody specific for Ago2. Cells transfected with miR-33a mimics had a higher expression of miR-33a in the RISC than cells transfected with control mimic (CM) or miR-33a* (Fig. 1G). Similarly, cells transfected with miR-33a* showed increased expression of miR-33a* in the RISC compared with cells transfected with CM or miR-33a (Fig. 1G). Altogether, these results demonstrate that we were able to determine specifically the expression of mature miR-33a and -a* and miR-33b and -b* and that these miRNAs are expressed in most human tissues.

Because miRNA and miRNA* sequences tend to show different patterns of nucleotide divergence (29–31), we next assessed

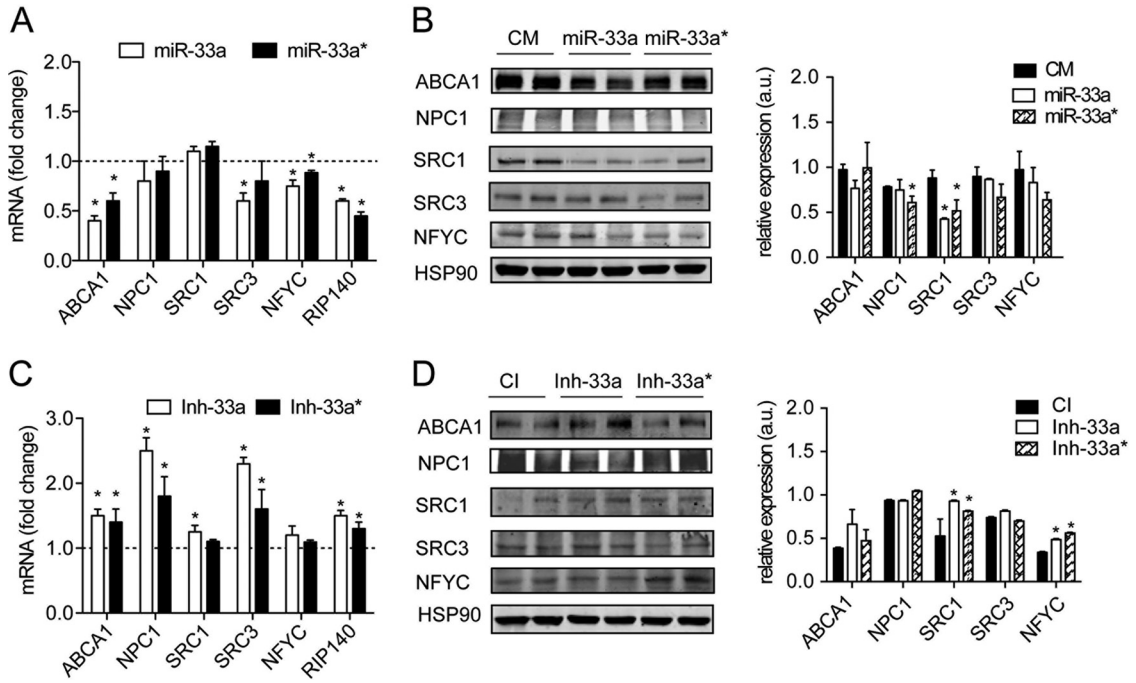

FIG 5 Posttranscriptional regulation of ABCA1, NPC1, SRC1, SRC3, NFYC, and RIP140 by miR-33a and miR-33a* in THP1 cells. (A) qRT-PCR analysis of ABCA1, NPC1, SRC1, SRC3, NYFC, and RIP140 in THP1 cells transfected with a control mimic (CM), miR-33a mimic, or miR-33a* mimic. (B) Western blot analysis of ABCA1, NPC1, SRC1, SRC3, and NFYC in THP1 cells transfected with CM, miR-33a, or miR-33a*. Quantification of protein relative to the loading control (HSP90) is shown in the right panel. (C) qRT-PCR analysis of ABCA1, NPC1, SRC1, SRC3, NYFC, and RIP140 in THP1 cells transfected with a control inhibitor (CI), inhibitor of miR-33a (Inh-33a), or inhibitor of miR-33a* (Inh-33a*). (D) Western blot analysis of ABCA1, NPC1, SRC1, SRC3, and NFYC in THP1 cells transfected with CI, Inh-33a, or Inh-33a*. Quantification of protein relative to the loading control (HSP90) is shown in the right panel. In panels A to D, the data are means ± SEM and representative of ≥3 experiments in triplicate. *, $P \leq 0.05$.

the evolutionary profiles of miR-33a and -a* and miR-33b and -b* in 21 vertebrate genomes. As shown in Fig. S1A in the supplemental material, both arms of the miR-33a duplex are highly conserved across vertebrates, while the conservation of miR-33b and -b* is lost in rats and mice (see Fig. S1B). Consistent with this, both miR-33 duplex arms were detectable in human hepatic cells (Huh7) and were synchronously expressed with their host genes, *Srebp-1* and *Srebp-2*, upon transcriptional activation (Fig. 2A and B). To ascertain whether both arms of the miR-33a duplex were coexpressed *in vivo*, C57BL/6 mice were fed a chow, high-fat diet (HFD) or statin-supplemented diet for 3 weeks. As shown in Fig. 2C, both miR-33a and miR-33a* were downregulated in the livers of mice fed the HFD and significantly upregulated in the livers of mice fed a diet supplemented with statin. Because the conservation of miR-33b in the intron of *Srebp-1* is lost in mice, we next evaluated the expression of miR-33b and -b* in the livers of rhesus monkeys stimulated with glucose. Intraperitoneal injection of a bolus of glucose to fasted monkeys led to peak glucose (174 ± 10 nM/liter) and insulin (8.9 ± 0.19 ng/ml) concentrations 5 and 15 min after injection, respectively. Consistent with this, SREBP-1 mRNA levels increased 60 min after glucose stimulation (Fig. 2D). Interestingly, both arms of the miR-33b duplex also increased after stimulation, suggesting for the first time that miR-33b or -b* is cotranscribed with its host gene *in vivo*. Thus, given that both miR-33a* and miR-33b* were concurrently expressed with their host genes *in vitro* and *in vivo*, we hypothesized that both passenger strands may be contributing to the endogenous role of the miR-33a/miR33b duplex.

miR-33 and miR-33* are predicted to regulate a similar number of target genes. To gain insight into the function of miR-33*, we analyzed its potential gene targets using the target prediction algorithm miRWalk (which provides target interaction information from eight different prediction programs, including miRanda, miRDB, and TargetScan) (32) and the pathway analysis tool Reactome (www.reactome.org). These prediction tools revealed that both miR-33a and -b duplex arms were enriched in lipid and specifically fatty acid metabolism ($P = 0.00088$ and 0.00039 for miR-33a and -a* and $P = 0.0028$ and 0.035 for miR-33b and -b*) and previously identified as direct targets of miR-33a and -b. Importantly, several genes involved in cellular cholesterol mobilization (*Abca1* and *Npc1*), fatty acid metabolism (*Cs* [coding for citrate synthase], *Crot*, *Cpt1a*, and *Ampk*α), and insulin signaling (*Irs2*) had putative binding sites for miR-33a* and -b*. In addition, several transcriptional regulators of lipid metabolism genes (*Src1*, *Src3*, *Rip140*, and *Nfyc*) were also predicted to be targets of both passenger strands (Tables 1 and 2).

miR-33* species can repress targets via perfect and near-perfect seed matches. To test whether miR-33a* and -b* could repress the *Abca1*, *Npc1*, *Cs*, *Crot*, *Cpt1a*, *AMPK*α, *Irs2*, *Src1*, *Src3*, and *Nfyc* genes, we used reporter constructs with the luciferase coding sequence fused to the 3′ UTR of the aforementioned genes. The constructs were cotransfected into COS7 cells along with a miR-33 mimic, miR-33* mimic, or nontargeting control mimic (CM). Similar to its sister strand, miR-33a* significantly inhibited the 3′-UTR activities of *Npc1*, *Irs2*, *Crot*, *Src1*, *Src3*, and *Nfyc* (see Fig. S2A B, and D to G in the supplemental material). Interest-

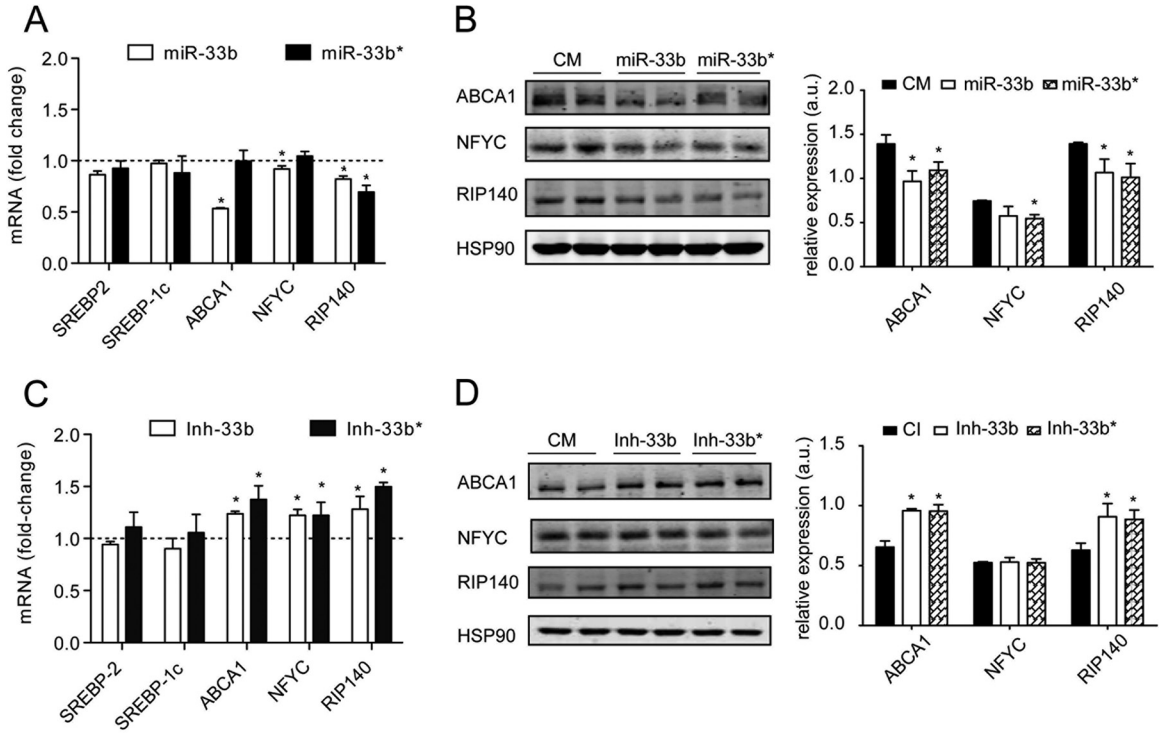

FIG 6 Posttranscriptional regulation of ABCA1, NFYC, and RIP140 by miR-33b and miR-33b* in Huh7 cells. (A) qRT-PCR analysis of SREBP-2, SREBP-1c, ABCA1, RIP140, and NFYC in Huh7 cells transfected with a control mimic (CM), miR-33b mimic, or miR-33b* mimic. (B) Western blot analysis of ABCA1, RIP140, and NFYC in Huh7 cells transfected with CM, miR-33b, or miR-33b*. Quantification of protein relative to the loading control (HSP90) is shown in the right panel. (C) qRT-PCR analysis of SREBP-2, SREBP-1c, ABCA1, RIP140, and NFYC in Huh7 cells transfected with a control inhibitor (CI), inhibitor of miR-33b (Inh-33b), or inhibitor of miR-33b* (Inh-33b*). (D) Western blot analysis of ABCA1, RIP140, and NFYC in Huh7 cells transfected with CI, Inh-33b, or Inh-33b*. Quantification of protein relative to the loading control (HSP90) is shown in the right panel. In panels A to D, the data are means ± SEM and representative of ≥3 experiments in triplicate. *, $P \leq 0.05$.

ingly, only miR-33a significantly inhibited the 3′ UTR of *Ampkα* and *Cpt1a*, despite binding sites for both duplex strands of miR-33a (see Fig. S2C and H). Transfection of miR-33b* resulted in reduced luciferase expression for *Nfyc* compared to controls (see Fig. S2J), while *Src3* 3′-UTR activity was unaffected (see Fig. S2K). Neither miR-33b nor miR-33b* repressed relative luciferase levels when cells were cotransfected with the 3′ UTR of *Cs* (see Fig. S2L). Notably, both miR-33* arms of miR-33a and -b failed to target *Abca1* 3′-UTR activity, despite strong downregulation from each sister strand (see Fig. S2I and M). Importantly, mutation of the miR-33a* and -b* target sites relieved the repression of *Npc1*, *Crot*, *Irs2*, *Src1*, *Src3*, and *Nfyc* (Fig. 3A to G) 3′-UTR activity, confirming a direct interaction of miR-33a* and -b* with these sites. Specifically, mutation of both miR-33a* sites in the 3′ UTR of *Src1* and *Src3* was needed to completely reverse the inhibitory effects of miR-33a* (Fig. 3D and E). To further determine the direct effect of miR-33a and -a* on some of their common target genes, we performed Ago2 immunoprecipitation in Huh7 cells transfected with miR-33a and miR-33a* and assessed the expression of CROT and NCP1 mRNA. Interestingly, the expression of CROT and NPC1 was increased in cells transfected with miR-33a and miR-33a* compared with that of cells that overexpressed a negative-control mimic (CM), suggesting that both miRNAs interact directly with CROT and NPC1 in the RISC (Fig. 3H).

miR-33 and miR-33* cooperate to regulate target gene repression. Although miR-33a and miR-33b have identical seed sequences, their sister strands are predicted to bind to different regions in the 3′ UTR of target genes (see Fig. S1 in the supplemental material). To determine whether miR-33a and -a* and miR-33b and -b* cooperate to reduce target gene expression, we tested the effect of each miRNA duplex on the 3′ UTR of several targets (*Npc1*, *Crot*, and *Nfyc*). Cotransfection of both miR-33a and miR-33a* resulted in a 10% further reduction of *Npc1*, *Crot*, and *Nfyc* 3′-UTR activity (data not shown). A similar effect was observed when COS7 cells were cotransfected with the 3′ UTR of *Nfyc* and a miR-33b and miR-33b* mimic (data not shown), thus suggesting that both arms of the miR-33a/miR-33b duplex may cooperate to regulate the expression of *Npc1*, *Crot*, and *Nfyc*.

miR-33* regulates gene expression in human macrophage and hepatic cell lines. We next determined whether miR-33a* and -b* could mediate translational repression of ABCA1, NPC1, CROT, CPT1a, IRS2, SRC1, SRC3, NFYC, and RIP140. Transfection of hepatic cells (Huh7) with miR-33a* significantly reduced NPC1, CPT1a, SRC1, and RIP140 mRNA and NPC1, CROT, CPT1a, IRS2, SRC1, SRC3, NFYC, and RIP140 protein expression, while *Srebp-2*, the host gene of miR-33a*, was unchanged (Fig. 4A and B). The repressive effects of miR-33a* were comparable to that of its sister strand, miR-33a (Fig. 4A and B), and were also reproduced in the human macrophage cell line THP1 (Fig. 5A and B), indicating that both arms of the miR-33a/miR-33a* duplex are active in these cell types. Consistent with this, overexpression of miR-33b* in Huh7 (Fig. 6A and B) and THP1 (Fig. 7A and

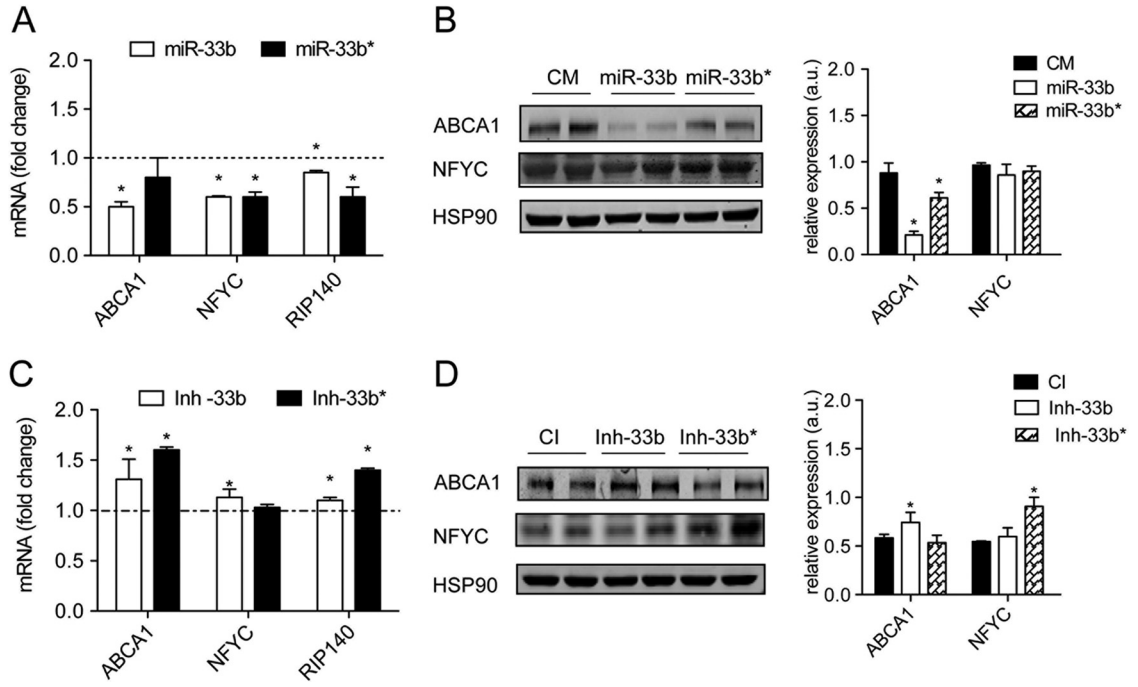

FIG 7 Posttranscriptional regulation of ABCA1, NFYC, and RIP140 by miR-33b and miR-33b* in THP1 cells. (A) qRT-PCR analysis of ABCA1, NYFC, and RIP140 in THP1 cells transfected with a control mimic (CM), miR-33b mimic, or miR-33b* mimic. (B) Western blot analysis of ABCA1 and NFYC in THP1 cells transfected with CM, miR-33b, or miR-33b*. Quantification of protein relative to the loading control (HSP90) is shown in the right panel. (C) qRT-PCR analysis of ABCA1, NYFC, and RIP140 in THP1 cells transfected with a control inhibitor (CI), inhibitor of miR-33b (Inh-33b), or inhibitor of miR-33b* (Inh-33b*). (D) Western blot analysis of ABCA1 and NFYC in THP1 cells transfected with CI, Inh-33b, or Inh-33b*. Quantification of protein relative to the loading control (HSP90) is shown in the right panel. In panels A to D, the data are means ± SEM and representative of ≥3 experiments in triplicate. $^*P \leq 0.05$.

B) cells also significantly decreased the mRNA expression of RIP140 and NFYC. Interestingly, both miR-33a* and miR-33b* strongly repressed ABCA1 and CPT1a expression in Huh7 (Fig. 4 and 6) and THP1 (Fig. 5 and 7) cells, despite confirmation of direct binding by luciferase assays (see Fig. S2 in the supplemental material). As SRC1 is a coactivator of ABCA1 expression (33) and a direct target of miR-33a*, we hypothesize that miR-33* is repressing ABCA1 mRNA and protein expression through this pathway. Similarly, PPARα, a transcriptional activator of CPT1a (34), also has a strong binding site for miR-33a* in its 3′ UTR, which may explain the repressive effects of miR-33a* on CPT1a mRNA and protein levels. Additionally, the moderate downregulation observed when we analyzed the effect of miR-33a* or miR-33b* on 3′-UTR activity compared with protein expression might be explained by the presence of canonical and noncanonical binding sites for both miRNAs within the coding regions of the target genes analyzed (data not shown). Indeed, several reports, using HITS-CLIP and PAR-CLIP, have shown that around 40% of miRNA binding sites are mapped to the coding region of certain genes (35, 36). Therefore, we cannot rule out that part of the effect of miR-33a* and miR-33b* might be due to certain binding activity on the coding region. Nevertheless, our present data show that at least a portion of their targeting activity is mediated through the binding sites located within the 3′ UTR of the analyzed genes. Further experiments are necessary to determine the biological significance of the miR-33a* and miR-33b* binding sites within mRNA coding regions. To assess the role of endogenous miR-33a* and -b* in regulating target gene expression, Huh7 and THP1 cells were transfected with a control inhibitor (CI), an inhibitor of miR-33a* (Inh-33a*), or an inhibitor of miR-33b* (Inh-33b*). As shown in panels C and D of Fig. 4, 5, 6, and 7, inhibition of endogenous miR-33a* or miR-33b* significantly increased the mRNA or protein levels of ABCA1, NPC1, CROT, CPT1a, SRC1, SRC3, NFYC, and RIP140, consistent with the hypothesis that miR-33a* and -b* have physiological roles in controlling lipid metabolism gene expression.

miR-33 and miR-33* differentially regulate target gene expression. To evaluate which miR-33 duplex arm plays a larger role in regulating lipid metabolism genes, we used lentiviral vectors to manipulate the levels of pre-miR-33a in human hepatic cells. Huh7 cells were efficiently transduced with a miR-33a lentiviral vector or empty control vector (Fig. 8A and B) and maintained green fluorescent protein expression after being cultured for 2 days (Fig. 8A). Moreover, miR-33-transduced cells presented increased levels of miR-33a and miR-33a* (Fig. 8C), as well as a concomitant decrease in expression of the genes coding for ABCA1, NPC1, CROT, CPT1a, IRS2, SRC1, SRC3, RIP140, and NFYC (Fig. 8D). Interestingly, transduced hepatic cells mimicked the ratio of miR-33 to miR-33* expression seen in human liver tissue (Fig. 1D). After confirmation of efficient transduction, Huh7 cells were transfected with an inhibitor of each duplex strand (Inh-33a and Inh-33a*) or control inhibitor (CI) and target gene expression was analyzed via qRT-PCR and Western blotting. As seen in Fig. 8E and F, both arms of the miR-33a duplex contribute to the repression of target genes, as inhibition of either miR-33a or miR-33a* led to the derepression of ABCA1, NPC1, CROT, CPT1a, IRS2, SRC1, SRC3, RIP140, and NFYC at the mRNA and protein level. Interestingly, miR-33a* seems to play a

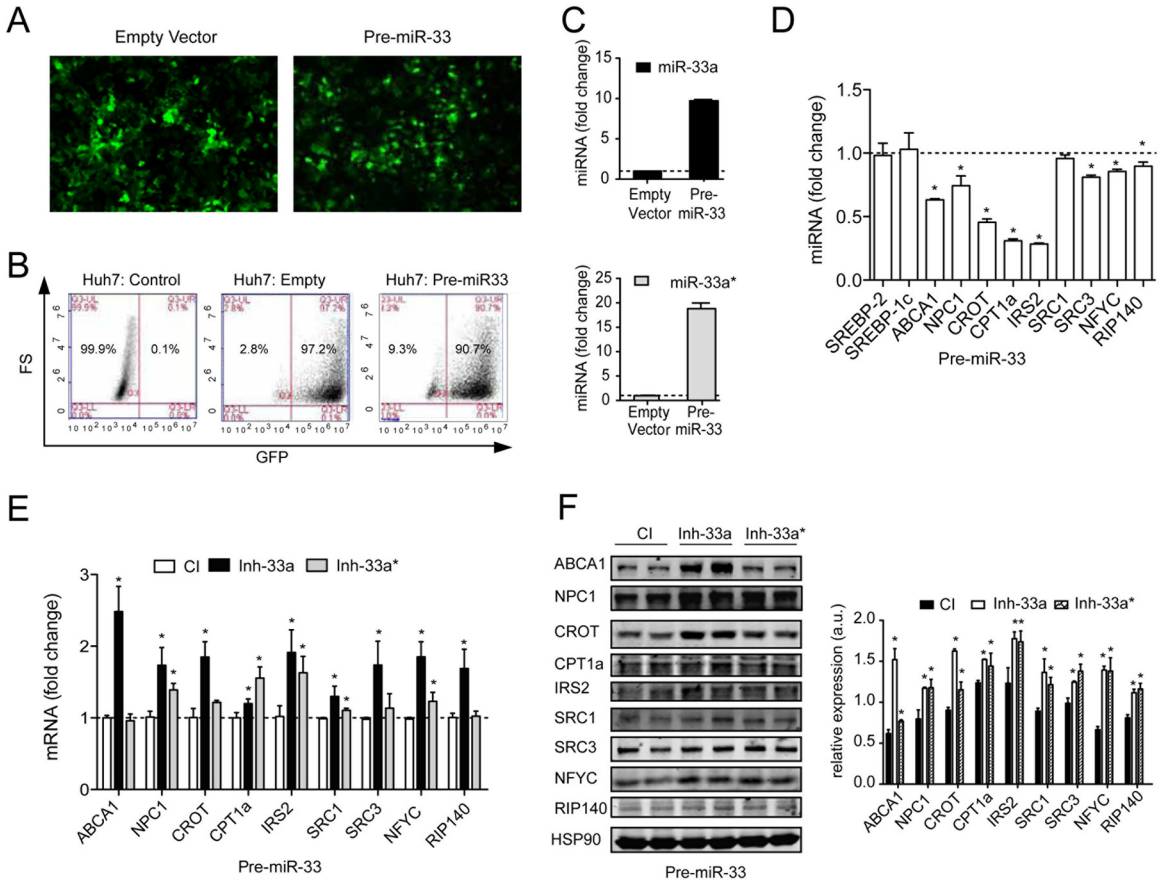

FIG 8 Both arms of the miR-33 duplex contribute to the posttranscriptional regulation of target gene expression. (A to B) Huh7 cells were transduced with a lentivirus encoding the miR-33a precursor (pre-miR-33) or empty vector control. Transduction efficiency was confirmed 48 h after culturing by measuring GFP expression using fluorescence microscopy (A) and flow cytometry (B). (C) qRT-PCR analysis of miR-33a (top panel) and miR-33a* (bottom panel) in empty vector-transduced or pre-miR-33-transduced Huh7 cells. (D) qRT-PCR analysis of SREBP-2, SREBP-1c, ABCA1, NPC1, CROT, CPT1a, IRS2, SRC1, SRC3, RIP140, and NFYC in Huh7 cells transduced with pre-miR-33. Values were compared to those from empty vector-transduced cells. (E) qRT-PCR analysis of ABCA1, NPC1, CROT, CPT1a, IRS2, SRC1, SRC3, RIP140, and NFYC in pre-miR-33-transduced Huh7 cells transfected with a control inhibitor (CI), inhibitor of miR-33a (Inh-miR-33a), or inhibitor of miR-33a* (Inh-miR-33a*). (F) Western blot analysis of ABCA1, NPC1, CROT, CPT1a, IRS2, SRC1, SRC3, NFYC, and RIP140 in pre-miR-33-transduced Huh7 cells transfected with CI, Inh-miR-33a, or Inh-miR-33a*. Quantification of protein relative to the loading control (HSP90) is shown in the right panel. FS, forward scatter. In panels A to F, the data are means ± SEM and representative of ≥2 experiments in triplicate. *, $P \leq 0.05$.

larger role in regulating CPT1a, NPC1, SRC3, and NFYC, as Huh7 cells transfected with Inh-33a* show a larger derepression at the protein level compared with Inh-33a (Fig. 8E). Taken together, these findings suggest a shared regulation of lipid metabolism by miR-33a and miR-33a*.

miR-33* inhibits cellular fatty acid oxidation. As miR-33* strongly inhibits several genes involved in fatty acid oxidation (coding for CROT and CPT1a), we next sought to investigate the functional role of miR-33* in this process. To this end, we evaluated the effects of miR-33a, miR-33a*, or miR-33a and -a* on fatty acid oxidation in Huh7 cells incubated with oleic acid for 12 h (Fig. 9A) and then starved for the next 24 h. As seen in Fig. 9C, Huh7 cells transfected with an miR-33a or miR-33a* mimic showed significantly lower levels of β-hydroxybutyrate, an end product of hepatic fatty acid oxidation (37), than cells transfected with a control mimic (CM). Interestingly, cells transfected with both miR-33a and miR-33a* showed slightly lower levels of β-hydroxybutyrate compared to cells transfected with either mimic alone, thus suggesting a shared regulation of fatty acid oxidation by both arms of the miR-33a/miR-33a* duplex. We next evaluated lipid droplet formation in Huh7 cells transfected with CM, miR-33a, or miR-33a*. Consistent with decreased levels of fatty acid oxidation, miR-33a- and miR-33a*-transfected cells accumulated significantly more triglycerides (TG) (Fig. 9D) and free fatty acids (FFA) (Fig. 9E) in larger lipid droplets (Fig. 9B).

DISCUSSION

The experiments shown herein expand our current understanding of how miR-33a and -b contribute to the regulation of lipid homeostasis. We and others have previously established that miR-33a and -b work in concert with their host genes, *Srebp-2* and *Srebp-1*, to ensure that a cell's metabolic state is balanced (18, 19, 21–23). During transcriptional activation of *Srebp-1* and *Srebp-2*, miR-33a and miR-33b are also transcribed, negatively regulating the expression of genes involved in cellular cholesterol export, fatty acid oxidation, and insulin signaling. We now show that the passenger strands of miR-33a and -b, miR-33a* and -b*, are also coincidentally generated with their host transcripts and repress

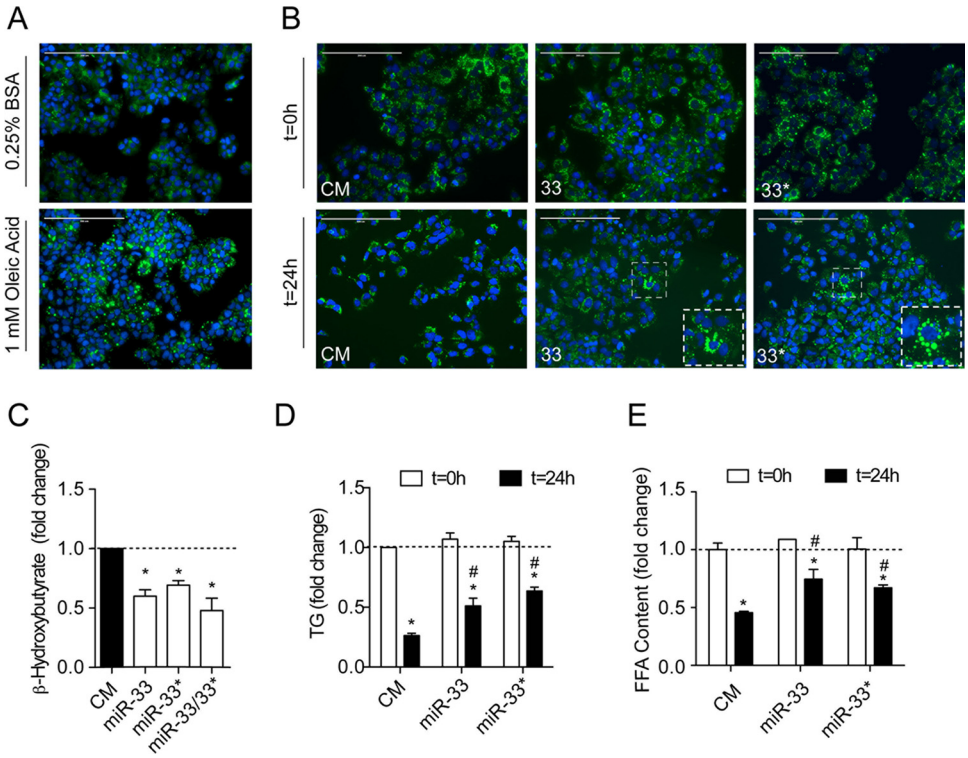

FIG 9 miR-33* cooperates with miR-33 to regulate fatty acid oxidation in human hepatic cells. (A) Neutral lipid accumulation in Huh7 cells loaded with 0.25% BSA or 1 mM oleic acid and stained with Bodipy (green) and DAPI (blue). Scale bar, 200 μm. (B) Neutral lipid accumulation in Huh7 cells transfected with a control mimic (CM), miR-33a mimic, or miR-33a* mimic and loaded with 1 mM oleic acid. Following 0 h and 24 h of starvation, cells were washed, fixed, and stained with Bodipy (green) and DAPI (blue). Scale bar, 200 μm. (C) Analysis of β-hydroxybutyrate in Huh7 cells transfected with CM, miR-33a, miR-33a*, or miR-33 and miR-33a* at 24 h of starvation. (D) Analysis of triglyceride (TG) content in Huh7 cells transfected with CM, miR-33a, or miR-33a* at 0 h and 24 h of starvation. (E) Analysis of free fatty acid (FFA) content in Huh7 cells transfected with CM, miR-33a or miR-33a* at 0 h and 24 h of starvation. In panels A to E, the data are means ± SEM and representative of ≥2 experiments in triplicate. *, $P \leq 0.05$ compared to CM (C) and compared to CM, miR-33, and miR-33* at time (*t*) 0 h (D and E). #, $P \leq 0.05$ compared to CM at 24 h (D and E).

similar genes involved in cholesterol export (*Abca1* and *Npc1*), fatty acid oxidation (*Crot* and *Cpt1a*), insulin signaling (*Irs2*), and the transcriptional regulation of lipid metabolism (*Src1*, *Src3*, *Rip140*, and *Nfyc*). Historically, miRNA* species contribute less to gene regulatory networks than their partner miRNA strands; however our data indicate that miR-33a* and -b* functionally contribute to the regulation of lipid homeostasis. We speculate that miR-33a* and -b* work collectively with their sister strands to boost intracellular cholesterol and fatty acid levels by balancing the posttranscriptional repression of genes involved in cellular cholesterol efflux and fatty acid oxidation. Given that miR-33a* and -b* have different seed sequences and share a similar target gene network with miR-33a and -b, accumulation of both arms of the miR-33 duplex would be predicted to (i) contribute to the posttranscriptional repression of similar transcripts through different sites in the target mRNA, and/or (ii) contribute to the posttranscriptional repression of distinct sets of mRNA transcripts in the same biological pathway (Fig. 10).

Thus far, relatively little is known about the functionality of miRNA* species. Signs of their existence arose with the development of deep sequencing techniques and were later followed by the demonstration of tissue-specific miRNA* abundance (8, 13). Hypothetically, each miRNA duplex produces an miRNA strand and miRNA* strand in a ratio that is predetermined by the thermodynamic stabilities and structural factors that contribute to miRNA accumulation (4, 5). Because each miRNA/miRNA* duplex has a unique structure and thermodynamic profile, these ratios should, in theory, remain constant across tissues (6). Our present study, however, suggests that the accumulation of miR-33a* and miR-33b* is tissue dependent, a finding that both challenges this hypothesis and extends recent reports of miRNA tissue-dependent stability. Indeed, while this article was in preparation, Voellenkle et al. reported a clear bias toward miR-33a* accumulation in endothelial cells using deep sequencing techniques (38). Additionally, it was reported that miR-33a* was not only expressed in monocyte-derived macrophages (MDMs), but also downregulated under M2-polarizing conditions (39). While these observations support our findings that miR-33* may contribute to the functional role of miR-33, the role of miR-33 in endothelial cells and MDMs is currently unknown.

The presence of miR-33a* and -b* in human, mouse, and nonhuman primate livers and their coexpression with *Srebp-2*, *Srebp-1*, and *miR-33a* and *-b* during cholesterol depletion or LXR stimulation *in vivo* strongly point towards a functionally active role for miR-33a* and -b* in regulating cholesterol and fatty acid metabolism. Here, we identify seven miR-33a* (*Npc1*, *Crot*, *Irs2*, *Src1*, *Src3*, *Nfyc*, and *Rip140*) and two miR-33b* (*Nfyc* and *Rip140*) target genes and show that miR-33a* and miR-33b* overexpression leads to their posttranscriptional repression. Notably, both miR-33a* and miR-33b* downregulate ABCA1 expression at the

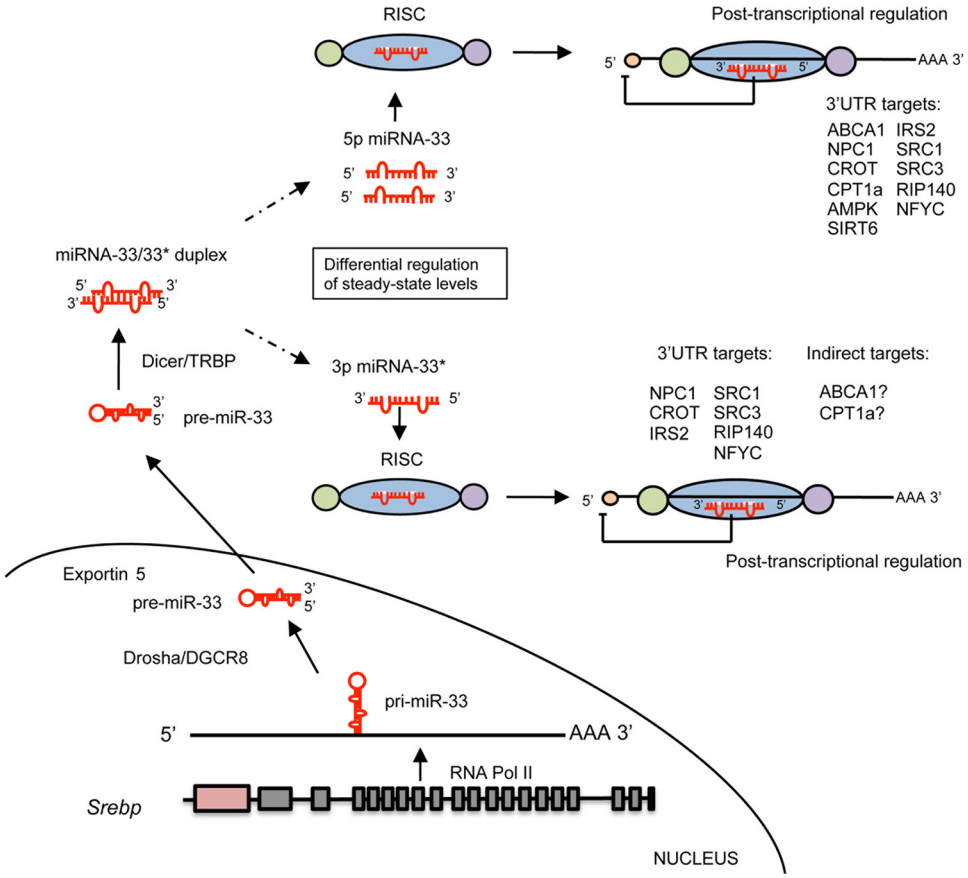

FIG 10 Proposed model of miR-33 arm-specific processing and target gene regulation. miR-33a* and -b* work collectively with their sister strands, miR-33a and -b, to boost intracellular cholesterol and fatty acid levels by balancing the posttranscriptional repression of genes involved in cellular cholesterol efflux (ABCA1 and NPC1), fatty acid oxidation (CROT, CPT1a, HADHB, and AMPK), glucose metabolism (SIRT6 and IRS2), and the transcriptional regulation of lipid metabolism (SRC1, SRC3, NFYC, and RIP140). Pol II, polymerase II.

mRNA and protein levels in human hepatocyte and macrophage cell lines, despite confirmation of direct binding. As SRC1 is a transcriptional activator of ABCA1 expression (33) and a direct target of miR-33a*, the downregulation of ABCA1 through this pathway cannot be ruled out. Unlike miR-33a*, miR-33b* does not directly target SRC1. Thus, we hypothesize that miR-33b* may be acting through an alternative mechanism. Indeed, miR-33b* has four predicted binding sites in the 3′ UTR of SP1, another transcriptional activator of ABCA1 expression. Taken together, these results point toward a shared regulation of ABCA1 expression by both arms of the miR-33/miR-33* duplex. One can imagine that during sterol-depleting states, when *Srebp-2* is transcriptionally activated to upregulate cholesterol uptake and synthesis genes, the miR-33/miR-33* duplex is also activated, downregulating ABCA1 expression directly through miR-33 or indirectly through the repression of ABCA1 transcriptional activators by miR-33*. Whether this has functional implications in regulating cholesterol efflux remains to be determined.

In addition to discovering novel targets for miR-33a* and -b*, our work also identifies miR-33a* as a functional regulator of fatty acid metabolism. By inhibiting the expression of CROT and CPT1a, miR-33a* reduces β-oxidation and concomitantly increases cellular free fatty acid levels and triglycerides in hepatocytes. In addition, luciferase activities indicate that miR-33a and miR-33a* synergistically regulate the expression of CROT, thus suggesting that both arms of the miR-33a duplex cooperate to regulate fatty acid oxidation. Indeed, overexpression of miR-33 and miR-33* in human hepatocytes led to a further reduction of β-oxidation than that in cells transfected with either mimic alone.

The present study corroborates recent reports indicating functional targets of specific mammalian miRNA* species, such as miR-223 and miR-223* (17) and miR-30e* (16), and supports the regulatory impact of miRNA* species on the mammalian genome. Together, these results raise the intriguing possibility that miR-33* plays a cooperative role with miR-33 by targeting the same transcripts within the Srebp axis, a key pathway for controlling cholesterol and fatty acid homeostasis. This is particularly relevant, as previous works from our lab and others have highlighted the therapeutic potential of inhibiting miR-33 to treat atherosclerosis and metabolic syndrome (40, 41). Because miR-33 and miR-33* have different seed sequences, inhibition of one duplex arm would not inhibit the functionality of the other arm. In fact, blocking the targeting of miR-33 could presumably lead to an increased loading of miR-33* into the RISC, especially given the shared regulation of target gene expression (42). Although this suggests that antagonism of miR-33* would enhance the seemingly beneficial effects of anti-miR-33 treatment, further studies are warranted to assess the functional contribution of miR-33* *in vivo*. Addition-

ally, experiments performed with primary mouse hepatocytes (for miR-33a and -a*) and human hepatocytes (for miR-33a and a* and miR-33b and -b*) will be important to define the roles of the guide and passenger strands in regulating lipid metabolism gene expression after physiological stimuli, such as insulin.

ACKNOWLEDGMENTS

This work was supported by the National Institutes of Health (R01HL107953 and R01HL106063 to C.F.-H., R01HL105945 to Y.S., and 1F31AG043318-01 to L.G.), the American Heart Association (12POST9780016 to C.M.R.), and the Deutsche Forschungsgemeinschaft (to D.C.-S.). Rafael de Cabo and Julie A. Mattison are supported by the Intramural Research Program of the NIH, National Institute of Aging.

REFERENCES

1. **Bartel DP.** 2009. MicroRNAs: target recognition and regulatory functions. Cell **136**:215–233.
2. **Ambros V.** 2004. The functions of animal microRNAs. Nature **431**:350–355.
3. **Filipowicz W, Bhattacharyya SN, Sonenberg N.** 2008. Mechanisms of post-transcriptional regulation by microRNAs: are the answers in sight? Nat. Rev. Genet. **9**:102–114.
4. **Khvorova A, Reynolds A, Jayasena SD.** 2003. Functional siRNAs and miRNAs exhibit strand bias. Cell **115**:209–216.
5. **Schwarz DS, Hutvagner G, Du T, Xu Z, Aronin N, Zamore PD.** 2003. Asymmetry in the assembly of the RNAi enzyme complex. Cell **115**:199–208.
6. **Mah SM, Buske C, Humphries RK, Kuchenbauer F.** 2010. miRNA*: a passenger stranded in RNA-induced silencing complex? Crit. Rev. Eukaryot. Gene Expr. **20**:141–148.
7. **Yang JS, Phillips MD, Betel D, Mu P, Ventura A, Siepel AC, Chen KC, Lai EC.** 2011. Widespread regulatory activity of vertebrate microRNA* species. RNA **17**:312–326.
8. **Okamura K, Phillips MD, Tyler DM, Duan H, Chou YT, Lai EC.** 2008. The regulatory activity of microRNA* species has substantial influence on microRNA and 3′ UTR evolution. Nat. Struct. Mol. Biol. **15**:354–363.
9. **Czech B, Malone CD, Zhou R, Stark A, Schlingeheyde C, Dus M, Perrimon N, Kellis M, Wohlschlegel JA, Sachidanandam R, Hannon GJ, Brennecke J.** 2008. An endogenous small interfering RNA pathway in Drosophila. Nature **453**:798–802.
10. **Czech B, Zhou R, Erlich Y, Brennecke J, Binari R, Villalta C, Gordon A, Perrimon N, Hannon GJ.** 2009. Hierarchical rules for Argonaute loading in Drosophila. Mol. Cell **36**:445–456.
11. **Schulte JH, Marschall T, Martin M, Rosenstiel P, Mestdagh P, Schlierf S, Thor T, Vandesompele J, Eggert A, Schreiber S, Rahmann S, Schramm A.** 2010. Deep sequencing reveals differential expression of microRNAs in favorable versus unfavorable neuroblastoma. Nucleic Acids Res. **38**:5919–5928.
12. **Okamura K, Liu N, Lai EC.** 2009. Distinct mechanisms for microRNA strand selection by Drosophila Argonautes. Mol. Cell **36**:431–444.
13. **Ro S, Park C, Young D, Sanders KM, Yan W.** 2007. Tissue-dependent paired expression of miRNAs. Nucleic Acids Res. **35**:5944–5953.
14. **Chiang HR, Schoenfeld LW, Ruby JG, Auyeung VC, Spies N, Baek D, Johnston WK, Russ C, Luo S, Babiarz JE, Blelloch R, Schroth GP, Nusbaum C, Bartel DP.** 2010. Mammalian microRNAs: experimental evaluation of novel and previously annotated genes. Genes Dev. **24**:992–1009.
15. **Goff LA, Davila J, Swerdel MR, Moore JC, Cohen RI, Wu H, Sun YE, Hart RP.** 2009. Ago2 immunoprecipitation identifies predicted microRNAs in human embryonic stem cells and neural precursors. PLoS One **4**:e7192. doi:10.1371/journal.pone.0007192.
16. **Jiang L, Lin C, Song L, Wu J, Chen B, Ying Z, Fang L, Yan X, He M, Li J, Li M.** 2012. MicroRNA-30e* promotes human glioma cell invasiveness in an orthotopic xenotransplantation model by disrupting the NF-kappaB/IkappaBalpha negative feedback loop. J. Clin. Invest. **122**:33–47.
17. **Kuchenbauer F, Mah SM, Heuser M, McPherson A, Ruschmann J, Rouhi A, Berg T, Bullinger L, Argiropoulos B, Morin RD, Lai D, Starczynowski DT, Karsan A, Eaves CJ, Watahiki A, Wang Y, Aparicio SA, Ganser A, Krauter J, Dohner H, Dohner K, Marra MA, Camargo FD, Palmqvist L, Buske C, Humphries RK.** 2011. Comprehensive analysis of mammalian miRNA* species and their role in myeloid cells. Blood **118**:3350–3358.
18. **Rayner KJ, Suarez Y, Davalos A, Parathath S, Fitzgerald ML, Tamehiro N, Fisher EA, Moore KJ, Fernandez-Hernando C.** 2010. MiR-33 contributes to the regulation of cholesterol homeostasis. Science **328**:1570–1573.
19. **Najafi-Shoushtari SH, Kristo F, Li Y, Shioda T, Cohen DE, Gerszten RE, Naar AM.** 2010. MicroRNA-33 and the SREBP host genes cooperate to control cholesterol homeostasis. Science **328**:1566–1569.
20. **Horton JD, Goldstein JL, Brown MS.** 2002. SREBPs: activators of the complete program of cholesterol and fatty acid synthesis in the liver. J. Clin. Invest. **109**:1125–1131.
21. **Marquart TJ, Allen RM, Ory DS, Baldan A.** 2010. miR-33 links SREBP-2 induction to repression of sterol transporters. Proc. Natl. Acad. Sci. U. S. A. **107**:12228–12232.
22. **Horie T, Ono K, Horiguchi M, Nishi H, Nakamura T, Nagao K, Kinoshita M, Kuwabara Y, Marusawa H, Iwanaga Y, Hasegawa K, Yokode M, Kimura T, Kita T.** 2010. MicroRNA-33 encoded by an intron of sterol regulatory element-binding protein 2 (Srebp2) regulates HDL in vivo. Proc. Natl. Acad. Sci. U. S. A. **107**:17321–17326.
23. **Davalos A, Goedeke L, Smibert P, Ramirez CM, Warrier NP, Andreo U, Cirera-Salinas D, Rayner K, Suresh U, Pastor-Pareja JC, Esplugues E, Fisher EA, Penalva LO, Moore KJ, Suarez Y, Lai EC, Fernandez-Hernando C.** 2011. miR-33a/b contribute to the regulation of fatty acid metabolism and insulin signaling. Proc. Natl. Acad. Sci. U. S. A. **108**:9232–9237.
24. **Gerin I, Clerbaux LA, Haumont O, Lanthier N, Das AK, Burant CF, Leclercq IA, MacDougald OA, Bommer GT.** 2010. Expression of miR-33 from an SREBP2 intron inhibits cholesterol export and fatty acid oxidation. J. Biol. Chem. **285**:33652–33661.
25. **Ho PC, Chang KC, Chuang YS, Wei LN.** 2011. Cholesterol regulation of receptor-interacting protein 140 via microRNA-33 in inflammatory cytokine production. FASEB J. **25**:1758–1766.
26. **Chamorro-Jorganes A, Araldi E, Penalva LO, Sandhu D, Fernandez-Hernando C, Suarez Y.** 2011. MicroRNA-16 and microRNA-424 regulate cell-autonomous angiogenic functions in endothelial cells via targeting vascular endothelial growth factor receptor-2 and fibroblast growth factor receptor-1. Arterioscler. Thromb. Vasc. Biol. **31**:2595–2606.
27. **Ramirez CM, Davalos A, Goedeke L, Salerno AG, Warrier N, Cirera-Salinas D, Suarez Y, Fernandez-Hernando C.** 2011. MicroRNA-758 regulates cholesterol efflux through posttranscriptional repression of ATP-binding cassette transporter A1. Arterioscler. Thromb. Vasc. Biol. **31**:2707–2714.
28. **Cheloufi S, Dos Santos CO, Chong MM, Hannon GJ.** 2010. A Dicer-independent miRNA biogenesis pathway that requires Ago catalysis. Nature **465**:584–589.
29. **Griffiths-Jones S, Hui JH, Marco A, Ronshaugen M.** 2011. MicroRNA evolution by arm switching. EMBO Rep. **12**:172–177.
30. **Guo L, Lu Z.** 2010. The fate of miRNA* strand through evolutionary analysis: implication for degradation as merely carrier strand or potential regulatory molecule? PLoS One **5**:e11387. doi:10.1371/journal.pone.0011387.
31. **Yang JS, Maurin T, Robine N, Rasmussen KD, Jeffrey KL, Chandwani R, Papapetrou EP, Sadelain M, O'Carroll D, Lai EC.** 2010. Conserved vertebrate mir-451 provides a platform for Dicer-independent, Ago2-mediated microRNA biogenesis. Proc. Natl. Acad. Sci. U. S. A. **107**:15163–15168.
32. **Dweep H, Sticht C, Pandey P, Gretz N.** 2011. miRWalk–database: prediction of possible miRNA binding sites by "walking" the genes of three genomes. J. Biomed. Inform. **44**:839–847.
33. **Huuskonen J, Fielding PE, Fielding CJ.** 2004. Role of p160 coactivator complex in the activation of liver X receptor. Arterioscler. Thromb. Vasc. Biol. **24**:703–708.
34. **Brandt JM, Djouadi F, Kelly DP.** 1998. Fatty acids activate transcription of the muscle carnitine palmitoyltransferase I gene in cardiac myocytes via the peroxisome proliferator-activated receptor alpha. J. Biol. Chem. **273**:23786–23792.
35. **Chi SW, Zang JB, Mele A, Darnell RB.** 2009. Argonaute HITS-CLIP decodes microRNA-mRNA interaction maps. Nature **460**:479–486.
36. **Hafner M, Landthaler M, Burger L, Khorshid M, Hausser J, Berninger P, Rothballer A, Ascano M, Jr, Jungkamp AC, Munschauer M, Ulrich A, Wardle GS, Dewell S, Zavolan M, Tuschl T.** 2010. Transcriptome-wide

identification of RNA-binding protein and microRNA target sites by PAR-CLIP. Cell **141**:129–141.
37. **Nabeshima Y, Tazuma S, Kanno K, Hyogo H, Chayama K.** 2009. Deletion of angiotensin II type I receptor reduces hepatic steatosis. J. Hepatol. **50**:1226–1235.
38. **Voellenkle C, Rooij J, Guffanti A, Brini E, Fasanaro P, Isaia E, Croft L, David M, Capogrossi MC, Moles A, Felsani A, Martelli F.** 2012. Deep-sequencing of endothelial cells exposed to hypoxia reveals the complexity of known and novel microRNAs. RNA **18**:472–484.
39. **Graff JW, Dickson AM, Clay G, McCaffrey AP, Wilson ME.** 2012. Identifying functional microRNAs in macrophages with polarized phenotypes. J. Biol. Chem. **287**:21816–21825.
40. **Rayner KJ, Esau CC, Hussain FN, McDaniel AL, Marshall SM, van Gils JM, Ray TD, Sheedy FJ, Goedeke L, Liu X, Khatsenko OG, Kaimal V, Lees CJ, Fernandez-Hernando C, Fisher EA, Temel RE, Moore KJ.** 2011. Inhibition of miR-33a/b in non-human primates raises plasma HDL and lowers VLDL triglycerides. Nature **478**:404–407.
41. **Rayner KJ, Sheedy FJ, Esau CC, Hussain FN, Temel RE, Parathath S, van Gils JM, Rayner AJ, Chang AN, Suarez Y, Fernandez-Hernando C, Fisher EA, Moore KJ.** 2011. Antagonism of miR-33 in mice promotes reverse cholesterol transport and regression of atherosclerosis. J. Clin. Invest. **121**:2921–2931.
42. **Biasiolo M, Sales G, Lionetti M, Agnelli L, Todoerti K, Bisognin A, Coppe A, Romualdi C, Neri A, Bortoluzzi S.** 2011. Impact of host genes and strand selection on miRNA and miRNA* expression. PLoS One **6**:e23854. doi:10.1371/journal.pone.0023854.